

Confrontation of Salammbô predictions of the storm-time electron belt population to in situ Strv/REM measurements

M. Kruglanski¹, D. Boscher², P. Bühler³ and D. Heynderickx¹

¹ *Belgian Institute for Space Aeronomy, B-1180 Brussels, Belgium*

² *DESP ONERA/CERT, F-31055 Toulouse, France*

³ *Paul Scherrer Institute, CH-5232 Villigen PSI, Switzerland*

Measurements of the Radiation Environment Monitor aboard the Strv-1b satellite have been confronted with the results of the Salammbô-3D code for the period of time from 5 to 18 April '95. Shortcomings of the current state of the Salammbô model are discussed.

INTRODUCTION

The prediction of the electron radiation belt dynamics during storm periods is an important issue in space weather forecasting. The Radiation Environment Monitor (REM) aboard the Strv-1B satellite in GTO orbit provides a wealth of data for studying the radiation environment and evaluating empirical and theoretical models of the radiation belts. The REM detector [Bühler *et al.*, 1996] is composed of two independent shielded silicon diodes measuring the linear energy transfer of charged particles. The shielding consists in each case of a dome of aluminium, but one diode has an additional shielding of tantalum. The combination of the signals from both detectors allows the determination of electron fluxes in three energy bins ranging from 1 to 10 MeV. The typical accumulation time is of the order of 100 seconds.

From June '94 to September '98, the REM instrument was in operation aboard the Strv-1b satellite, launched into a highly elliptical GTO orbit with apogee and perigee altitude of 300 km and 36000 km, respectively, a period of about 10 hours, and inclination of 7 degrees. The orbit passes repeatedly through the Earth radiation belts. The Strv-1b/REM data set [Bühler *et al.*, 1999] therefore provides a good coverage of the equatorial part of the radiation belts over a period of four years. Due to the high spin rate of the satellite with respect to the accumulation time and the large opening angle of the detector, only omnidirectional fluxes are obtained from the Strv-1b/REM measurements. Due to the limited data storage capacity aboard Strv-1b, REM was not continuously operated, so that some orbits are missing. Parts of the Strv-1b/REM data have already been analysed in other studies, e.g. by Bühler *et al.* [1999], Desorgher *et al.* [1997, 1998] and Daly *et al.* [1999].

DESP (*Département d'Étude Spatiale*) has developed the Salammbô-3D code [Beutier and Boscher, 1995] to simulate the radiation belt dynamics by solving a classical Fokker-Planck diffusion equation in the (M, J, L^*) space as a function of time. In the framework of the ESA/ESTEC TREND contract, Salammbô-3D results have been confronted to in situ data for several magnetic storms during two periods of time for which sufficient data were

available. The first period corresponds to the CRRES mission for which data from the Meteosat-3, GOES-6 and GOES-7 spacecraft are also available. Comparisons between CRRES/MEA measurements [Vampola *et al.*, 1992] and Salammbô-3D simulations have been used to include and tune a temporal variation of the radial diffusion coefficients and of the plasmopause location into the Salammbô model. The final results for the four storms studied during this period show good agreement between measurements and simulations [Boscher and Bourdarie, 1999].

In order to evaluate the generality of the adaptations, we have applied the code with the same tuning to a second period. The second period corresponds to the conjunction of the Strv-1b, Meteosat-3, GOES-7 and WIND missions and extends from April '94 to December '95.

Four storms occurring during this period were studied. In this paper, we only report on the comparison for the period 5–18 April '95. This period covers a storm associated with a fast solar wind stream, with good data availability from Strv-1b/REM but also from the SEM-2 instrument aboard Meteosat-3, from GOES-7 and from WIND. The GOES and WIND data were not used during the computations but are important for the understanding and interpretation of the results. The Meteosat-3/SEM-2 instrument [Coates *et al.*, 1991] provides electron flux measurements in 5 energy channels between 43 and 300 keV at geostationary orbit. The SEM-2 measurements have been used to determine the boundary conditions of the Fokker-Planck equation during the studied period. The Strv-1b/REM data are confronted with Salammbô-3D to evaluate the Salammbô capabilities to reproduce the dynamics of electrons in an energy range higher than the CRRES/MEA range (0.12–1.7 MeV). The Strv-1b data are not used to define the initial condition.

The Salammbô-3D model and its different ingredients used for the simulation are described in the first section. The second section is dedicated to the confrontation between Strv-1b/REM measurements and Salammbô results. The results are not as good as for the CRRES period; possible shortcomings are discussed in the third section. The conclusions are given in the last section.

1. MODELLING THE 7 APRIL STORM

1.1. Description of the Salammbô-3D model

The Salammbô-3D model is the first of a series of numerical codes developed by DESP to study the dynamics of the Earth radiation belts. It is based on the solution of a classical Fokker-Planck diffusion equation in the three adiabatic invariants M , J , L^* : the magnetic moment, the second action integral and Roederer's [1970] magnetic shell parameter, respectively. The ingredients needed for such a diffusion model are particle sources, transport and loss processes, and also the initial and boundary conditions.

For electrons, the Salammbô-3D model does not include explicit sources inside the radiation belts. The only source is localised at the boundary $L^* = 7$ of the model, and thus corresponds to storm and substorm injections.

Figure 1

The particle transport is assumed to be due only to Coulomb interaction with neutral atoms or cold electrons, to wave interactions and to electromagnetic fluctuations. The Coulomb interaction occurs with neutrals from the exosphere or cold electrons from the plasmasphere. It is evaluated with the help of an eccentric tilted dipole magnetic field (the coefficients of which are evaluated from the IGRF models), the exosphere neutral model MSIS-86 and the model for plasmaspheric electrons of *Carpenter and Anderson [1992]*. The Coulomb interaction is used in Salammbô with yearly averaged parameters to calculate a friction term and pitch angle diffusion coefficients. Wave interactions related to plasmaspheric hiss, whistlers and VLF transmitters are also used to evaluate pitch angle diffusion coefficients. The evaluation of the wave interactions makes use of the *Abel and Thorne [1998]* calculations and of a plasmopause location r_p related to the maximum value of K_p in the preceding day by the *Carpenter and Anderson [1992]* formula

$$r_p = 5.6 - 0.46 K_{pmax}. \quad (1)$$

Electromagnetic fluctuations inside the magnetosphere lead to radial diffusion and their classical coefficients. To adapt the radial diffusion to the magnetic activity, the radial diffusion coefficients have been multiplied by the factor

$$g = e^{0.74 K_p} \quad (2)$$

[*Bourdarie et al., 1996; Boscher et al., 1998*].

Most of the losses occur in the loss cone where particles are precipitated mostly by pitch angle diffusion. The loss regions are thus located at the boundaries of the Salammbô model, where the electron fluxes are forced to zero. Internal losses are included as well by taking synchrotron losses into account [*Pugacheva et al., 1998*].

1.2. Application of Salammbô-3D

To apply Salammbô-3D, the conditions at the different boundaries have to be determined. At the inner edge, the electron fluxes were forced to zero to take into account the absorption by the atmosphere. At the outer edge, defined by $L^* = 7$, the electron fluxes were set to measured values based on the Meteosat-3/SEM-2 data provided by MSSL [*Lemaire et al., 1995*]; note that McIlwain's [1961] L for the Meteosat-3 orbit varies between 6.8 and 7.4 when evaluated with the IGRF 1995 geomagnetic field model and the *Olson and Pfitzer [1977]* quiet external magnetic field model. Since Meteosat-3/SEM-2 covers only a limited energy range, the data are extrapolated down to 2.2 keV and up to 600 keV. The energy range is extended below 22 keV with the energy spectrum is obtained from ATS6 measurements [*Parks et al., 1977*]. Above 600 keV, the electron fluxes are forced to zero. Based on CRRES/MEB data [*Gussenhoven et al., 1985*], the pitch angle distribution is fixed at $L^* = 7$ to the power law $\sin^{3.32} \alpha_0$ at all energies. The Meteosat-3/SEM-2 flux data, available with a time

resolution of 500 s, allow to generate highly dynamical boundary conditions.

The energy range and resolution of the Strv-1b/REM data are too limited to set the initial conditions for a Salammbô-3D run. Therefore, the initial conditions from a run for the CRRES period are used (24 September 1991 [Boscher and Bourdarie, 1999]).

The Salammbô-3D model is run on a grid of $25 \times 25 \times 25$ points in (M, J, L^*) space, with a time step of 34 s. For analysis and presentation purposes, the results are projected on a grid of $9 \times 18 \times 21$ points in the (E, α_0, L^*) space, every 3 hours.

2. THE PERIOD 5–18 APRIL '95

The selected 13-day period beginning 5 April 1995 covers a magnetic storm that was initiated by a fast solar wind stream impinging upon the magnetosphere. The solar wind velocity was high and nearly constant during 4 days. The velocity and density of the solar wind for the 13-day period as observed by WIND are displayed on the top panels of Figure 1. After the shock, the GOES-7 data indicates a jump of the energetic $E > 2$ MeV electron flux at geostationary distance above $10^4 \text{ cm}^{-2}\text{s}^{-1}\text{sr}^{-1}$ which is maintained during 7 days (third panel of Figure 1). The electron flux even exceeds $10^5 \text{ cm}^{-2}\text{s}^{-1}\text{sr}^{-1}$, 3 days after the shock. The electron fluxes observed by the five energy channels of Meteosat-3/SEM-2 are also displayed on Figure 1, as well as the Meteosat-3 L values, K_p and D_{st} . The GOES-7 and Meteosat-3 spectra clearly show that at geostationary distance the flux enhancement occurs first at low energies and then at higher energies: the elapsed time between the changes at 50 keV and at 2 MeV is about 2 days.

In Figure 2, the measurements of the Strv-1b/REM instrument are presented for comparison with the results of the Salammbô simulation. The Strv-1b/REM data are ordered according to McIlwain's [1961] L evaluated with IGRF 1995 and the Olson and Pfitzer [1977] quiet model in the same way as the Meteosat-3 data. Except for 6 and 13 April, the Strv-1b/REM data provides a good spatial coverage of the radiation belts. The REM instrument is not capable of separating electrons and protons below $L = 2.5$. During the main phase of the magnetic storm, the electron fluxes are decreasing together with D_{st} everywhere in the outer belt. At the start of the recovery phase, the electron fluxes increase rapidly to higher values than before the storm onset. They continue to increase during the recovery phase, the fluxes continue to increase slowly. The dynamics of both Strv-1b/REM energy channels are very similar. The maximum flux is reached after 5 days at $L = 5.5$, and after 9 days at $L = 4$.

On panels 4 to 6 of Figure 2, unidirectional electron flux maps produced from Salammbô results are displayed: the 600 keV equatorial flux, the $L^* = 4$ equatorial energy spectrum and the $L^* = 4$ pitch angle distribution for 600 keV, respectively. The storm appears clearly with an increase of the electron fluxes during the recovery phase. The Salammbô simulation is thus able to reproduce the basic trend of the magnetic storm. However, the electron

Figure 2

dropout during the main phase of the storm does not seem to be simulated except at high L where it is probably forced by the boundary conditions. Part of this particle dropout can be related to the decrease of the magnetic field when the ring current is enhanced [Desorgher *et al.*, 1998] or during the growth phase of substorms [Sauvaud *et al.*, 1996].

In order to directly compare the Strv-1b/REM measurements and the Salammbô simulation, the Salammbô results have been integrated in energy and pitch angle to predict the REM measurements along the Strv-1b orbit. The result of the simulation of the 1.0–2.2 MeV Strv-1b/REM channel is presented on panel 7 of Figure 2. The simulated fluxes do not follow the measurements shown on the first panel: there are no significant variations in the Salammbô flux except at the end of the period for the lowest L values. For a more detailed comparison, the Salammbô predictions and Strv-1b/REM measurements are shown in Figure 3 for four Strv-1b orbits: one orbit before the storm, one orbit during the main phase and two orbits during the recovery phase. Before the storm, the measurements and predictions look similar in spite of Salammbô initial conditions being based on data from a different epoch. During the storm, the predicted electron fluxes do not decrease during the growth phase, as already observed on Figure 2, and Salammbô overestimates the REM flux by a factor 10. This can be partly due to the effect of L as the Strv-1b/REM measurements were plotted using a McIlwain L and a static magnetic field while the Salammbô results are obtained in (M, J, L^*) space. During the recovery phase, the differences between measurements and predictions become even more significant. Both measured and simulated fluxes increase in the outer belt region, but the shape, the growth rate and the amplitude are very different. For large L values the discrepancies are probably due to boundary conditions. As noted before, at $L^* = 7$ the fluxes above 600 keV are forced to zero. Moreover, as the electron acceleration is thought to be due to the recirculation process [Fujimoto and Nishida, 1990] —a phenomenon that is highly non-linear— comparisons are better for low energies than for higher one. The recirculation is a combined effect of radial and pitch angle diffusion, and neither processes adequately modelled.

Figure 3

3. SHORTCOMINGS OF THE SIMULATION

For the simulation of Strv-1b/REM measurements presented in Figures 2 and 3, the Salammbô-3D model has been applied without any fitting procedure to minimize the discrepancies between measurements and observation, even at the start of the period. The results therefore provide the opportunity to determine the strengths and weaknesses of this type of model in predicting the space environment for space weather applications. The success or failure of a simulation are related to:

- the availability of in situ measurements, especially the boundary conditions;
- the suitability of these data to derive initial and boundary conditions for the model, although the same initial conditions were used with success for different situations (see Figure 3 panel 1);

- the modelisation of the physical processes.

The availability of in situ measurements is probably the most important barrier to good-quality prediction tools. In our case, initial conditions were not available and experimental boundary conditions are limited to almost equatorially mirroring electrons of energies between 43 and 300 keV.

The limited energy range of the data used to determine the boundary conditions also strongly influences the results. Figure 4 shows the energy increases for equatorially mirroring electrons due to radial diffusion from $L^* = 7$. The energies at $L^* = 7$ correspond to the Meteosat-3/SEM energy channels. These particles only reach the energy levels of the Strv-1b/REM detector below $L^* = 4$. Therefore, the $E > 1$ MeV electron population is poorly affected by the magnetic storm in the Salammbô simulation when $L > 5$. This could probably explain a great part of the discrepancies between Salammbô results and Strv-1b/REM observations during the recovery phase.

Another shortcoming, related to the building of the initial and boundary conditions, is the reduction of the experimental data. In addition to the problem of the cross calibration between different experiments, we have also to associate the measurements to L and α_0 values in order to compare those measurements with the Salammbô-3D simulation. In our study, L is evaluated with the help of *McIlwain's* [1961] formula where the Earth's magnetic moment M_0 is fixed to 0.311653 G Re^3 , and α_0 is defined as

$$\sin^2 \alpha_0 = M_0 L^{-3} B_m^{-1}, \quad (3)$$

where B_m is the magnetic field intensity at the mirror point. As mentioned previously, the magnetic field model used to order the Strv-1b/REM and Meteosat-3/SEM data is static, i.e. it is not affected by the magnetic storm. On Figure 5, the L values used in our studies are compared to values obtained with the *Pfizer et al.* [1988] dynamic external magnetic field model for both Meteosat-3 and Strv-1b on 7 April 1995. The *Pfizer et al.* [1988] dynamic model depends on D_{st} and solar wind parameters. During the main phase, the differences between both L evaluations exceed one Earth radius for Meteosat-3 as well for Strv-1b. Using a dynamic magnetic field model will clearly affect the comparison between Salammbô results and Strv-1b measurements, especially during the main phase (second panel of Figure 3). But since the dynamic magnetic field model also causes L variation for Meteosat-3, it precludes a continuous determination of the boundary conditions near $L^* = 7$.

The last class of shortcoming is related to the modelisation of the physical processes acting in the magnetosphere. Some model parameters, e.g. the ionosphere high altitude densities, the magnetic and electric field fluctuations, or the wave characteristics, are not known well enough. The most uncertain coefficients are certainly the radial diffusion coefficients, which should depend on magnetic activity. In this simulation, this dependence is implemented only by an ad-hoc exponential on K_p (see Equation 2). The dynamics

Figure 4

Figure 5

of the magnetic field during periods of magnetic activity should also be included in the Salammbô-3D model. During the main phase of a magnetic storm, non-adiabatic modifications of the particle movement and energy occur: particles are subject to strong induced electric fields and can be lost by drifting into the magnetopause [Desorgher *et al.*, 1998; Desorgher, 1999].

4. CONCLUSIONS

The Salammbô-3D code is a powerful tool to analyse the radiation belt behaviour during high magnetic activity events. For electrons below 1 MeV, most of the physical phenomena occurring in the dynamics of their population seem to be modelled in the code, even if some model aspects have to be improved such as radial diffusion coefficients, wave spectrum and wave localization. The comparison with Strv-1b/REM measurements shows that Salammbô has to be improved in order to correctly simulate populations of very high energetic electrons, especially in the outer belt. In particular, an additional loss mechanism is needed at large L and the dependence of the radial diffusion on magnetic activity has to be enhanced.

The development of tools and models like Salammbô is restrained by the lack of in situ measurements. Continuous measurements on a broad energy spectrum should help to better understand the dynamics in the outer belt and to better identify the model shortcomings. The model development, as well as the comparison between predictions and measurements, is also affected by the way to define the L parameter. Different definitions of L can lead to differences greater than one Earth radius in the evaluation of L . This variation could clearly lead to misinterpretation of comparisons between theoretical models and experimental data.

Acknowledgements. This work was supported by ESA, Space Environments and Effects Major Axis, under ESTEC Contract No. 8011/88/NL/MAC.

REFERENCES

- Abel, B., and R. Thorne, Electron scattering loss in Earth's inner magnetosphere 1. Dominant physical processes, *J. Geophys. Res.* 103, 2385–2396, 1998
- Abel, B., and R. Thorne, Electron scattering loss in Earth's inner magnetosphere 2. Sensitivity to model parameters, *J. Geophys. Res.* 103, 2397–2407, 1998
- Beutier T., D. Boscher, and M. France, Salammbô: A three-dimensional simulation of the proton radiation belt, *J. Geophys. Res.* 100, 14853–14861, 1995.
- Boscher, D., and S. Bourdarie, Physical modelling of the outer belt high energy electrons, Workshop on Space Weather, Noordwijk (The Netherlands), 11–13 November 1998, ESTEC WPP-155, 411–414, 1999
- Bourdarie, S., D. Boscher, T. Beutier, J. Sauvaud, M. Blanc, and R. Friedel, A physics based model of the radiation belt flux at the day timescale, Symposium on Environment modelling for space-based applications, Noordwijk (The Netherlands), 18–20 September 1996, ESA SP-392, 159–163, 1996
- Boscher, D., S. Bourdarie, R. Friedel, and A. Korth, Long term dynamic for low energy protons, *Geophys. Res. Lett.*, 4129, 1998

- Bühler, P., S. Ljungfelt, A. Mchedlishvili, N. Schlumpf, A. Zehnder, L. Adams, E. Daly, and R. Nickson, Radiation environment monitor, Nucl. Instr. and Meth. in Phys. Res. A 368, 825–831, 1996.
- Bühler, P., L. Desorgher, A. Zehnder, and E. Daly, Observation of the radiation belts with REM, Workshop on Space Weather, Noordwijk (The Netherlands), 11–13 November 1998, ESTEC WPP-155, 333–337, 1999.
- Carpenter, D., and R. Anderson, An ISEE/whistler model of equatorial electron density in the magnetosphere, J. Geophys. Res. 97, 1097–1108, 1992.
- Coates, A., A. Johnstone, D. Rodgers, and G. Wrenn, Quest for the source of Meteosat anomalies, Proceedings of spacecraft charging technology conference 1989, ed R.C. Olsen, Naval Postgraduate School, Monterey (CA), 120–146, 1991.
- Daly E., P. Bühler, and M. Kruglanski, Observations of the outer radiation belt with REM and comparisons with models, IEEE Nuclear and Space Radiation Effects Conference, Norfolk, VA, 1999.
- Desorgher, L., Variations of the Earth's outer electron belt - REM observations between 1995 and 1997 and simulations of magnetic storm effects, Ph.D. thesis, Universität Bern (Switzerland), 1999.
- Desorgher, L., P. Bühler, A. Zehnder, E. Daly, L. Adams, Outer radiation belt losses during magnetic storm, Workshop Space Radiation Environment Modelling: New Phenomena and Approaches, Moscow (Russia), October 7–9, 1997.
- Desorgher, L., P. Bühler, E. Flückiger, A. Zehnder, E. Daly, L. Adams, Modelling of the outer electron belt during magnetic storms, 32nd COSPAR Scientific Assembly, Nagoya (Japan) 12–19 July 1998.
- Fujimoto, M., and A. Nishida, Energization and anisotropization of energetic electrons in the earth's radiation belts by the recirculation process, J. Geophys. Res. 95, 4265–4270, 1990.
- Gussenhoven, M., E. Mullen, and R. Sagalyn, CRRES/SPACERAD Experiment Descriptions, AFGL Tech. Rep. 85-0017, Hanscom AFB (Massachusetts), 1985.
- Lemaire, J., A. Johnstone, D. Heynderickx, D. Rodgers, S. Szita, and V. Pierrard, Trapped radiation environment model development TREND-2 - final report, Aeronomica Acta 393, 133–184, 1995.
- McIlwain, C. E., Coordinates for Mapping the Distribution of Magnetically Trapped Particles, J. Geophys. Res., 66, pp. 3681–3691, 1961.
- Olson, W. P., and K. A. Pfizter, Magnetospheric magnetic field modeling, Annual Scientific Report, AFOSR Contract No. F44620-75-C-0033, 1977.
- Parks, G., C. Lin, B. Mauk, S. DeForest, and C. McIlwain, Characteristics of magnetospheric particle injection deduced from events observed on August 18, 1974, J. Geophys. Res. 82, 5208–5214, 1977.
- Pfizer, K. A., W. P. Olson, and T. Mogstad, A time dependent source driven magnetospheric magnetic field model, EOS, 69, 426, 1988.
- Pugacheva G., A. Gusev, I. Martin, D. Boscher, S. Bourdarie, and W. Spjeldvik, Numerical modeling of magnetospheric electron radial transport with accounting synchrotron radiation losses, Geophys. Res. Lett. 25, 1519–1522, 1998.
- Roedere, J., Dynamics of geomagnetically trapped radiation, Springer-Verlag, New York, 106–111, 1970.
- Sauvaud, J., T. Beutier, and D. Delcourt, On the origin of flux dropouts near geosynchronous orbit during the growth phase of substorms 1. Betatron effects, J. Geophys. Res. 101, 19911–19919, 1996.
- Vampola, A., J. Osborn, and B. Johnson, The CRRES magnetic electron spectrometer, J. Spacecraft and Rockets 29, 592–594, 1992.

CAPTIONS

Figure 1. For the period from 5 to 18 April 1995, from top to bottom, the solar wind bulk velocity and density from WIND, the GOES-7 $E > 2$ MeV electron flux, the geostationary electron spectrum from Meteosat-3/SEM-2 and corresponding McIlwain's L , the K_p planetary index and the D_{st} magnetic activity index.

Figure 1. For the period from 5 to 18 April 1995, from top to bottom, the solar wind bulk velocity and density from WIND, the GOES-7 $E > 2$ MeV electron flux, the geostationary electron spectrum from Meteosat-3/SEM-2 and corresponding McIlwain's L , the K_p planetary index and the D_{st} magnetic activity index.

Figure 2. For the same period as Figure 1, the 1.0–2.2 and 2.2–4.6 MeV outer-belt electron fluxes from Strv-1b/REM as a function of L , the D_{st} magnetic activity index, the Salammbô-3D results including the L -distribution of 600 keV equatorially mirroring electron flux, the energy spectrum at $L = 4$ of equatorially mirroring electrons and the α_0 -distribution of 600 keV electron flux at $L = 4$, and the simulation of the Strv-1b/REM 1.0–2.2 MeV measurements from the Salammbô-3D results.

Figure 2. For the same period as Figure 1, the 1.0–2.2 and 2.2–4.6 MeV outer-belt electron fluxes from Strv-1b/REM as a function of L , the D_{st} magnetic activity index, the Salammbô-3D results including the L -distribution of 600 keV equatorially mirroring electron flux, the energy spectrum at $L = 4$ of equatorially mirroring electrons and the α_0 -distribution of 600 keV electron flux at $L = 4$, and the simulation of the Strv-1b/REM 1.0–2.2 MeV measurements from the Salammbô-3D results.

Figure 3. Comparison of 1.0–2.2 MeV electron flux observed by Strv-1b/REM (thick green curves) with the Salammbô-3D simulation of these measurements (thin red curves) along four orbits: one before the storm, one during the main phase and two during the recovery phase.

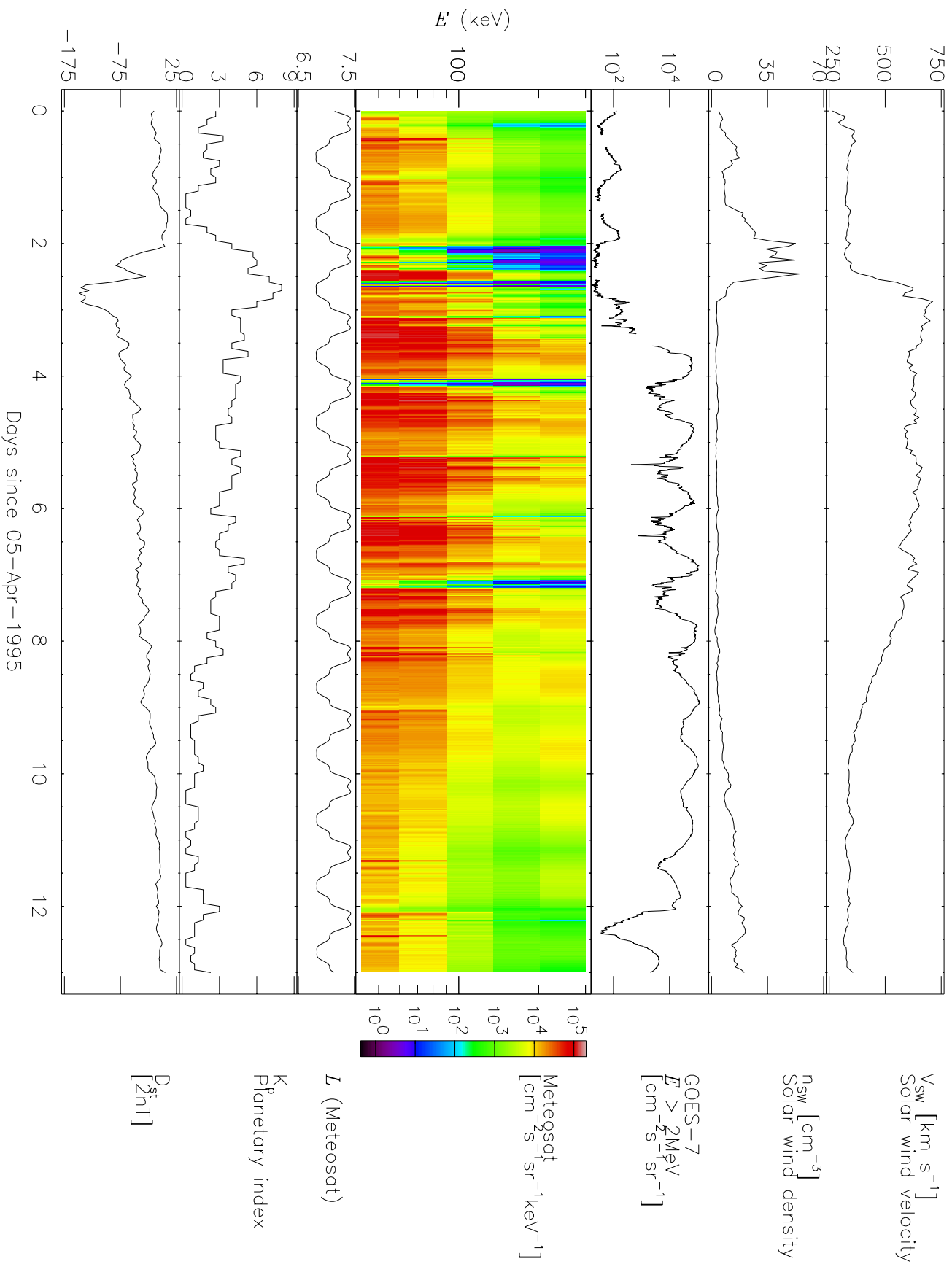
Figure 3. Comparison of 1.0–2.2 MeV electron flux observed by Strv-1b/REM (thick green curves) with the Salammbô-3D simulation of these measurements (thin red curves) along four orbits: one before the storm, one during the main phase and two during the recovery phase.

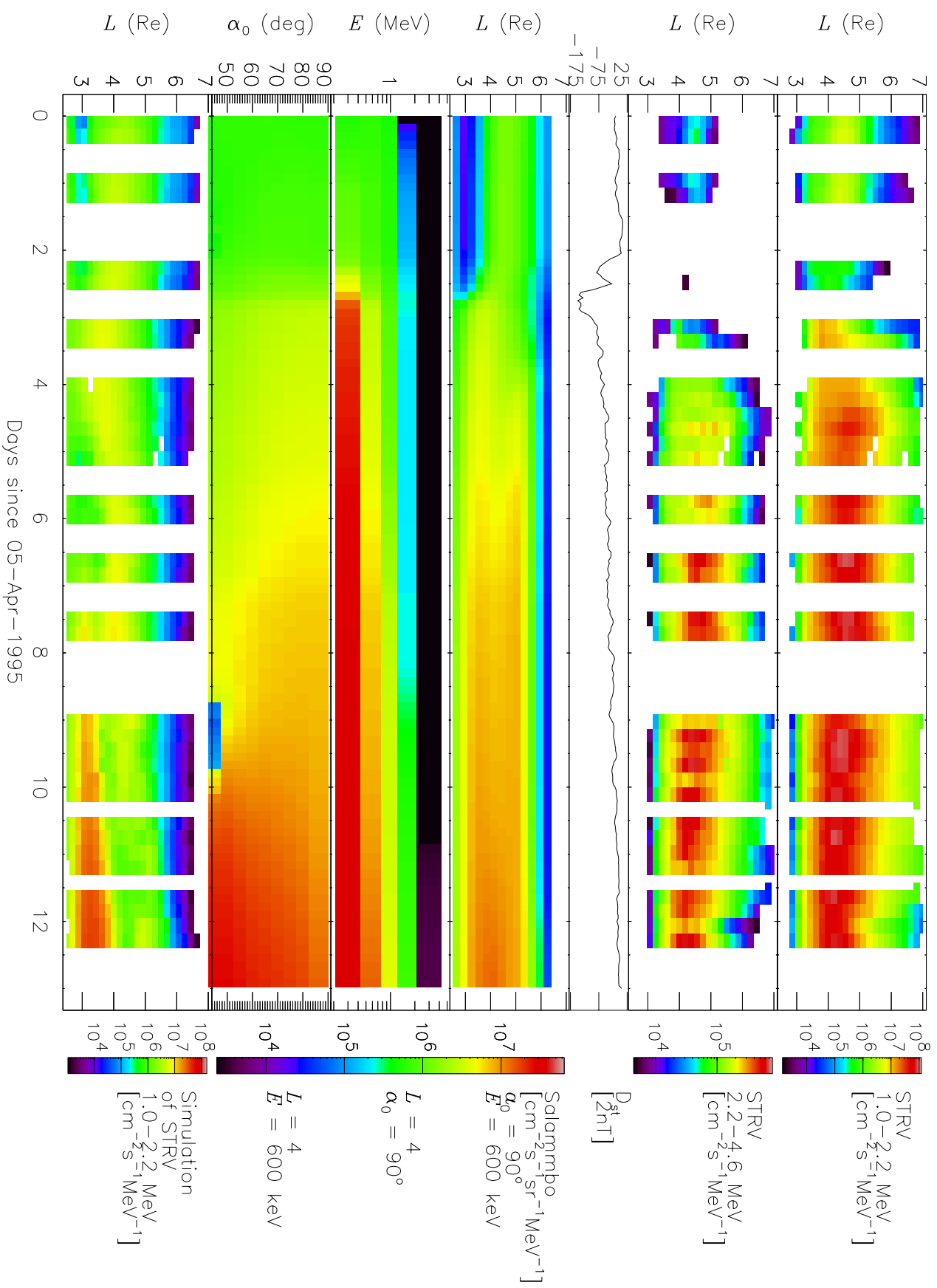
Figure 4. Illustration of the energy increases for equatorially mirroring electrons due to a pure radial diffusion from $L = 7$. The different curves correspond to the energy range of the five Meteosat-3/SEM-2 energy channels.

Figure 4. Illustration of the energy increases for equatorially mirroring electrons due to a pure radial diffusion from $L = 7$. The different curves correspond to the energy range of the five Meteosat-3/SEM-2 energy channels.

Figure 5. Evaluation of McIlwain's L for Meteosat-3 (top panel) and Strv-1b satellites on 7 April 1995 using two different external magnetic field models: the *Olson and Pfitzer [1977]* quiet model (green curves) and the *Pfitzer and Olson [1988]* dynamic model (red curves).

Figure 5. Evaluation of McIlwain's L for Meteosat-3 (top panel) and Strv-1b satellites on 7 April 1995 using two different external magnetic field models: the *Olson and Pfitzer [1977]* quiet model (green curves) and the *Pfitzer and Olson [1988]* dynamic model (red curves).





1.0–2.2 MeV Electron flux ($\text{cm}^{-2}\text{s}^{-1}$)

